Chemical Engineering Journal 336 (2018) 297–305

Contents lists available at ScienceDirect

Chemical Engineering Journal

journal homepage: www.elsevier.com/locate/cej

Chemically activated microporous carbons derived from petroleum coke: Performance evaluation for CF_4 adsorption

XiangZhou Yuan*[,1], Seung Wan Choi[1], Eunji Jang, Ki Bong Lee*

Department of Chemical and Biological Engineering, Korea University, 145 Anam-ro, Seongbuk-gu, Seoul 02841, Republic of Korea

ARTICLE INFO

Keywords:
CF_4 adsorption
Microporous carbon
KOH activation
Petroleum coke
Kinetics

ABSTRACT

CF_4 is considered to be a significant global-warming compound and has a fairly long atmospheric lifetime, which exacerbates climate change. Adsorption is considered a promising technology for capturing CF_4 and appropriate adsorbent is one of key factors for successful development of adsorption method. In this study, CF_4 adsorption using microporous carbon materials was investigated from both equilibrium and kinetic perspectives. Petroleum coke (PC) was utilized for developing CF_4 adsorbents by carbonization and KOH-activation processes. The carbonization temperature and KOH/PC mass ratio were varied from 300 to 600 °C and from 1 to 3, respectively. Varying the carbonization temperature and KOH/PC mass ratio had a dramatic effect on the textual properties of the prepared samples. CF_4 adsorption was well fitted by the Langmuir isotherm model, and the CF_4 uptake was remarkably dominated by the surface area and pore volume of narrow micropores below 0.8 nm in diameter. The experimental CF_4 adsorption data were well described by the pseudo-second-order kinetic model, compared with the Elovich and intra-particle-diffusion models, and CF_4 adsorption appeared to be mainly controlled by physisorption. The PC450-K2 adsorbent, prepared using a carbonization temperature of 450 °C and a KOH/PC mass ratio of 2, exhibited the highest CF_4 adsorption uptake of 2.79 mol kg^{-1} at 25 °C and 1 atm, in addition to good CF_4/N_2 selectivity at relatively low CF_4 pressures, excellent recyclability, easy regeneration, and rapid adsorption-desorption kinetics.

1. Introduction

Due to the continuing aggravation of global warming, considerable interest has been generated in reducing the atmospheric concentration of greenhouse gases, including carbon dioxide (CO_2), methane (CH_4), nitrous oxide (N_2O), chlorofluorocarbons (CFCs), hydrochlorofluorocarbons (HCFCs), hydrofluorocarbons (HFCs), and perfluorocarbons (PFCs) [1–4]. CO_2 accounts for 70% of total greenhouse-gas emissions and the current CO_2 level contributes to global warming and anthropogenic climate change; therefore, reducing the CO_2 level in the atmosphere is considered one of the most important environmental and scientific challenges [5,6]. There have been many studies on CO_2 capture, storage, and utilization (CCUS), and CO_2 separation from other gases, with developments discussed in detail in several recent reviews [7–12].

Reducing non-CO_2 greenhouse-gas emissions is now also considered important and is receiving more and more interest because the use of non-CO_2 greenhouse gases is increasing [13]. In particular, due to their high stability and low chemical reactivity, PFCs have been used in a wide range of applications, including in microelectronics for cleaning or printing electronic circuit boards, dry-etching processes in the semiconductor industry, and chemical vapor decomposition processes in aluminum production [14,15]. The simplest PFC, tetrafluoromethane (CF_4), is known to be a particularly powerful greenhouse gas and has an extremely long atmospheric lifetime of 50,000 years; consequently, CF_4 has 7390-times more global-warming potential than CO_2 over a 100-year period [16–19]. Therefore, several technologies have been developed in attempts to prevent CF_4 emission, including thermal combustion, plasma treatment, catalytic decomposition, and adsorption.

CF_4 capture based on adsorption technology is a simple and effective method, and activated carbons (ACs) are thought to be promising among the various applicable adsorbents [19]. ACs have found widespread use for adsorbing components from gaseous and liquid phases, as a result of their high specific surface area, large pore volume, well-developed microporosity, robustness, and long lifetime [20,21]. In addition, the low price of AC is highly desirable for practical environmental and energy-related applications. Among the many different precursors for AC, petroleum coke (PC) is advantageous because of its

* Corresponding authors.
E-mail addresses: yuan0125@korea.ac.kr (X. Yuan), kibonglee@korea.ac.kr (K.B. Lee).
[1] These authors contributed equally to this work.

https://doi.org/10.1016/j.cej.2017.11.168
Received 1 November 2017; Received in revised form 26 November 2017; Accepted 27 November 2017
Available online 28 November 2017
1385-8947/

Table 1
Comparison of previously reported adsorbents tested for CF_4 adsorption.

Sample name	Base material	S_{BET} ($m^2 g^{-1}$)	V_T ($cm^3 g^{-1}$)	q_e (25 °C, 1 atm)	Ref.
TiC-CDC800H	TiC powder	1749	0.80	2.96	[24]
AC	Carbosieve G	1100	0.56	1.68[a]	[25]
PBPC800	PVDF powder	991	0.43	1.85	[1]
MOF	$Zn_4O(dmcpz)_3$	n.a.	0.50	1.88	[26]
MOF	MIL-101	n.a.	n.a.	0.83	[27]
SWNTs	Nanotubes	n.a.	n.a.	2.40[b]	[28]
Zeolite 13X	Zeolite 13X	670	0.24	0.78[c]	[29]
ZSM-5-280	Zeolite-5A	n.a.	n.a.	1.31[a]	[30]

[a] At 23 °C and 1 atm.
[b] At 27 °C and 1 atm.
[c] At 30 °C and 1 atm.

cheapness and abundant production from oil refineries and, thus, PC was utilized for synthesizing a CF_4 adsorbent in this study. Generally, two different activation processes, physical and chemical, are adopted for making activated porous carbons from carbon precursors. The physical activation process is relatively environmentally friendly, but requires high temperatures and its porous-carbon yield is low. The chemical activation process consumes less energy due to its low operating temperature and short treatment time, and has the advantage of delivering high yield and a well-developed pore structure. The agents used in the chemical activation process, such as KOH, NaOH, $ZnCl_2$, and H_3PO_4, are corrosive and an additional washing step is needed to remove these chemicals from the produced porous carbon [22,23].

The few investigations on CF_4 adsorption that have been conducted are summarized in Table 1, and include the use of zeolite, metal-organic-framework (MOF), and AC adsorbents [1,24–30]. In this study, PC-derived porous carbons were prepared by chemical activation treatment using KOH and then evaluated for CF_4 adsorption for the first time. The carbonization temperature and KOH/PC mass ratio used in the treatment were varied from 300 to 600 °C and from 1 to 3, respectively. The morphology, structure, and textual properties of the PC-derived porous carbons were systematically characterized and their CF_4 adsorption behavior, including adsorption uptake, regenerability, cyclic stability, and adsorption-desorption kinetics, was studied in detail.

2. Materials and methods

2.1. Synthesis of KOH-activated PC

Petroleum coke (PC, obtained from Hyundai Oilbank, Republic of Korea) was used as a carbon precursor to develop a new CF_4 adsorbent. The PC was first crushed and pulverized to obtain particles with sizes of 180–425 μm. Proximate and ultimate analyses of PC were performed, with the results shown in Table 2.

PC-derived porous carbons for CF_4 adsorption were synthesized using two main steps: carbonization followed by KOH chemical activation. The pristine PC was first placed in a horizontal cylindrical furnace (50 mm inner diameter) and heated at a rate of 5 °C min^{-1} up to a predetermined temperature in the range of 300–600 °C under nitrogen flow (200 mL min^{-1}). The temperature was maintained for 1 h to achieve carbonization. The carbonized PC is denoted as PC*x*, where *x* is the carbonization temperature.

The KOH activation process was performed using the following steps: 1) 1 g of carbonized PC and 1–3 g of KOH were mixed in 5 mL of deionized water at 60 °C for 2 h; 2) this mixture was put into a drying furnace in order to remove the water and the dried sample was then placed in the horizontal cylindrical furnace at 700 °C for 1 h under nitrogen flow in order to produce pores in the carbonized PC; 3) the KOH-activated sample was washed several times with HCl and deionized water until the pH of the filtrate became neutral, and the sample was finally dried in a furnace at 110 °C for 24 h. The final KOH-activated sample is denoted PC*x*-K*y*, where *y* represents the KOH/PC mass ratio.

Table 2
Proximate and ultimate analyses of petroleum coke.

Analysis type		Content (wt%)
Proximate Analysis (ar†)	Moisture	0.39
	Volatile Matter	9.15
	Fixed Carbon	89.76
	Ash	0.70
Ultimate Analysis (daf‡)	C	85.28
	H	3.54
	O*	0.50
	N	1.22
	S	7.68

Note: †As-received (ar); ‡Dry-ash free basis (daf); *calculated by difference.

2.2. Sample characterization

Scanning electron microscopy (SEM, S-4800, Hitachi) and high-resolution transmission electron microscopy (HR-TEM, G2F30ST, Tecnai) were used to investigate the morphology of PC and PC*x*-K*y*. The textural properties of the samples were estimated using N_2 adsorption isotherm data at -196 °C obtained using a volumetric adsorption analyzer (ASAP 2020, Micromeritics). All samples were degassed at 150 °C under vacuum (10 μmHg) for 12 h before the N_2 adsorption isotherm measurements. Functional-group modification after the activation process was evaluated using Fourier transform infrared spectroscopy (FT-IR, Nicolet iS10, Thermo Scientific). The formation of defects and transition between sp^2 and sp^3 hybridization in the samples were confirmed using micro-Raman spectroscopy with the 532 nm line of a DPSS laser (Omicron) at room temperature, where the beam size at the sample was approximately 3 μm.

Dynamic CF_4 adsorption-desorption measurements and cyclic stability tests were performed using thermogravimetric analysis (TGA, Q50, TA Instruments) at 30 °C and atmospheric pressure. In the dynamic adsorption-desorption measurements, adsorption was performed in a CF_4 flow for 6 h, followed by desorption with a N_2 flow for 4 h. For the cyclic stability tests, ten adsorption-desorption cycles were repeated, with a single cycle consisting of CF_4 adsorption for 1 h and desorption with N_2 purging for 1.5 h. In addition, CF_4 adsorption tests were conducted using a volumetric adsorption analyzer (BELSORP-mini II, BEL Japan). Prior to the adsorption tests, the PC*x*-K*y* samples were degassed at 150 °C under vacuum for 10 h, and the adsorption isotherms were attained at three different temperatures of 25, 40, and 60 °C.

3. Results and discussion

3.1. Characteristics of KOH-activated PC carbonized at different temperatures

Fig. 1 shows SEM and HR-TEM images of the PC*x*-K*y* samples. There are no obvious differences between the SEM images of the different PC*x*-K*y* samples, and the HR-TEM image of PC450-K2 shows well-distributed pores with a size of less than 1 nm, indicating that the carbonization and activation processes produced well-developed micropores [31,32].

Fig. 2 shows FTIR spectra of the PC*x*-K*y* samples. The bands observed at 800 and 1380 cm^{-1} are attributed to the C—H bending vibration [33]. The bands at around 1100 and 1210 cm^{-1} are probably associated with the O—H, C—O, and C—O—C bending vibrations [34,35]. The peak at 1650 cm^{-1} corresponds to C═C stretching in aromatic rings that are conjugated with either another C═C bond, an aromatic nucleus, or a C═O bond; the C═C stretching frequently occurs at approximately 1650 cm^{-1} for carbonaceous materials [35–37].

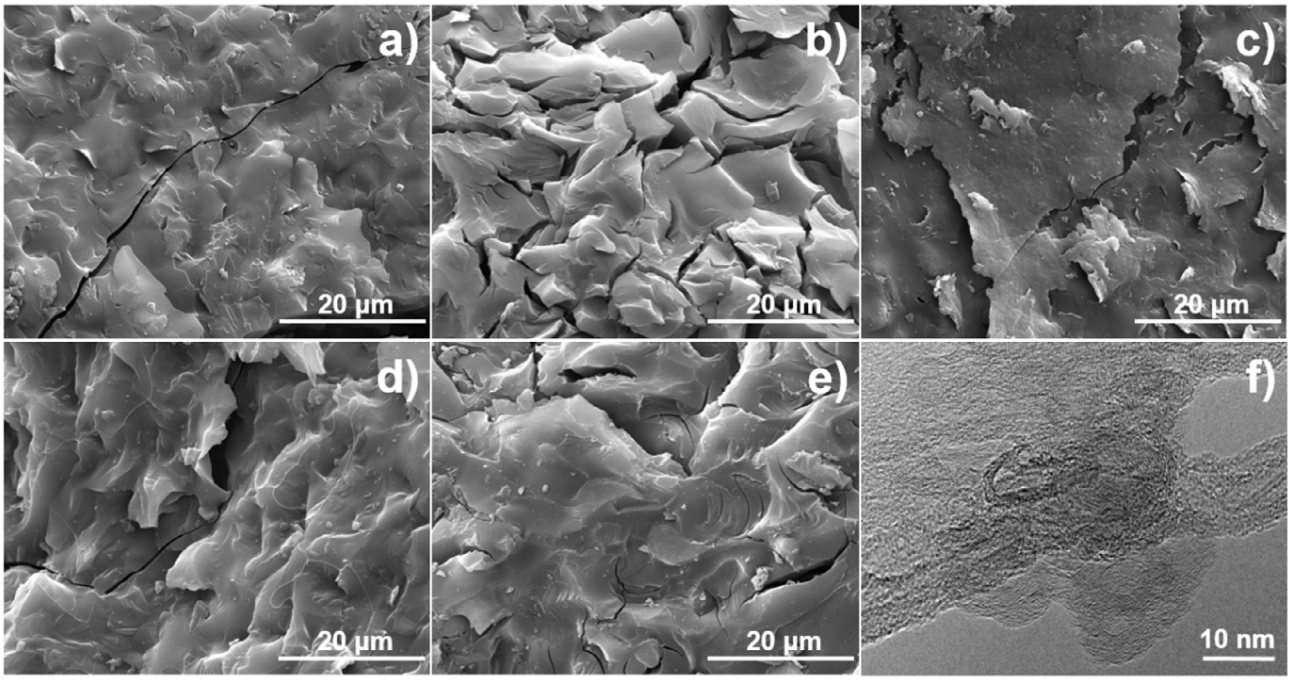

Fig. 1. SEM images of a) PC300-K2, b) PC600-K2, c) PC450-K1, d) PC450-K2, and e) PC450-K3. f) HR-TEM image of PC450-K2.

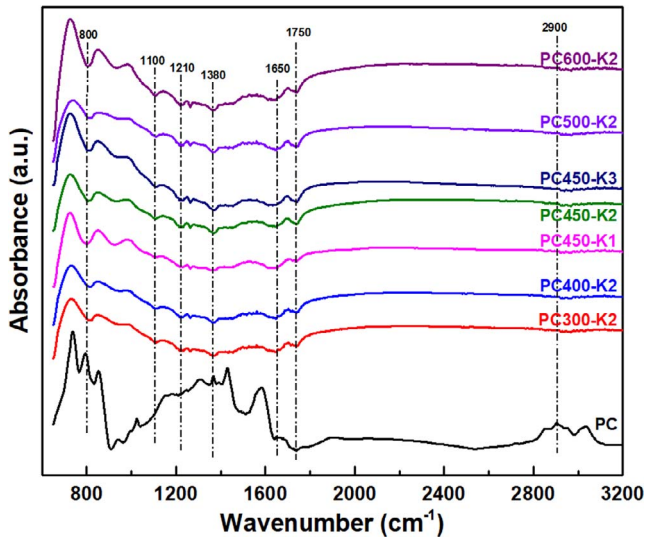

Fig. 2. FTIR spectra of PC and PC*x*-K*y* samples.

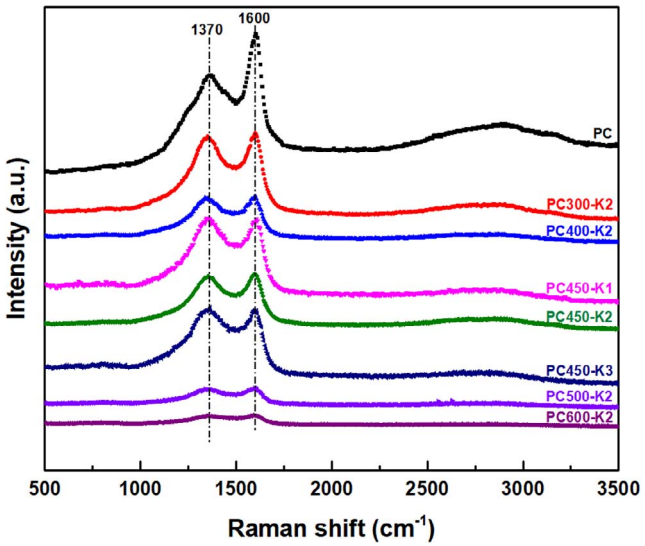

Fig. 3. Raman spectra of PC and PC*x*-K*y* samples.

There is a small peak at 1750 cm^{-1}, which is attributed to the C=O vibration of carboxylic and carbonyl groups [38]. The weak band at around 2900 cm^{-1} is assigned to asymmetric and symmetric C–H stretching vibrations on aliphatic groups, such as $-CH_2$, $-CH_3$, and $-CH_2CH_3$ [34,39], which are introduced by KOH during the chemical-activation process [40].

Raman spectra of the PC and PC*x*-K*y* samples are displayed in Fig. 3. The two distinct peaks at ~1370 and ~1600 cm^{-1} indicate that the samples possess highly amorphous structures. The peak at ~1370 cm^{-1} (D-band) is attributed to the breathing mode of κ-point phonons with A^{1g} symmetry, corresponding to disordered carbon or defective graphitic structures [41]. The peak at ~1600 cm^{-1} (G-band) is assigned to the E^{2g} phonon of sp^2 carbon atoms [42], which is a characteristic feature of graphitic layers and corresponds to tangential vibration of the carbon atoms [43]. The D-peak to G-peak intensity ratios (I_D/I_G) for the PC*x*-K*y* samples are greater than that for PC, indicating that the PC*x*-K*y* samples possess a well-developed porous structure.

Fig. 4 shows the N_2 adsorption-desorption isotherm behavior of PC*x*-K*y* at −196 °C. The N_2 adsorption isotherm can be categorized as type I according to the International Union of Pure and Applied Chemistry (IUPAC) classification, indicating that the prepared porous carbons are typical microporous materials [44]. The significant N_2 uptake clearly observed in the low-pressure region ($P/P_0 < 0.05$) is attributed to filling of the micropores with N_2 gas. The adsorption-desorption curves were identical, with no hysteresis loop. Fig. 4a shows that the N_2 uptake in the low-pressure region gradually increased with increasing carbonization temperature used for sample preparation from 300 to 450 °C, and then decreased with further increases in the carbonization temperature from 450 to 600 °C, which indicates a change in the microporosity. Fig. 4b shows that the N_2 uptake for PC450-K*y* dramatically increased with increasing KOH/PC mass ratio. On increasing the KOH/PC mass ratio to 3 (PC450-K3), the sharp knee in the PC450-K1 isotherm became wider, indicating that the micropores were enlarged.

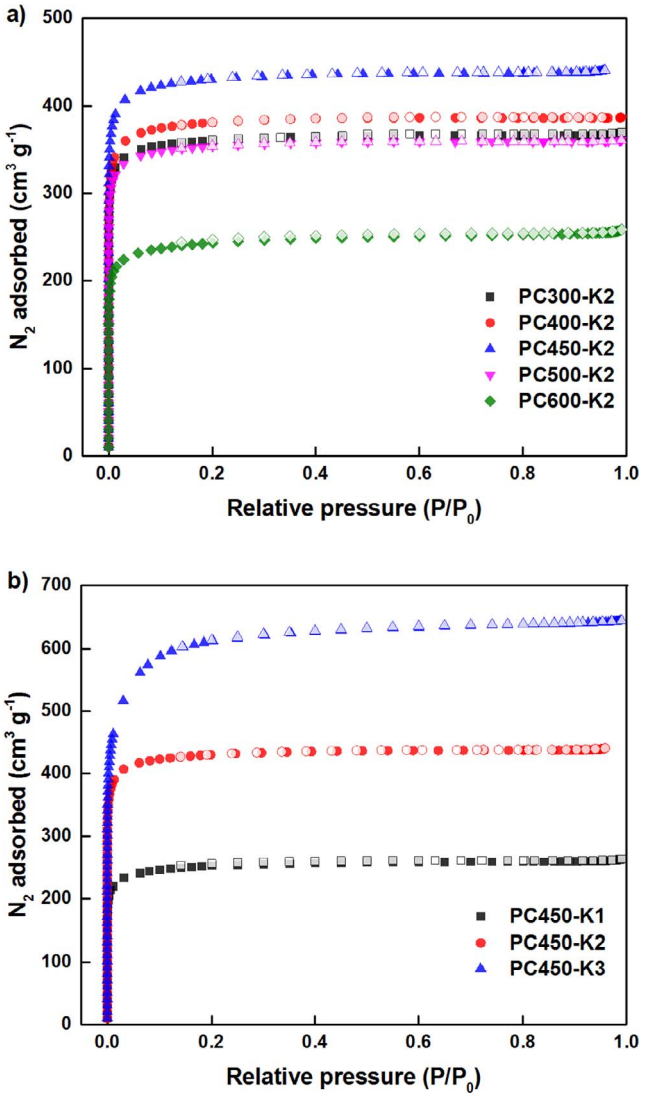

Fig. 4. N_2 adsorption (solid symbols) and desorption (open symbols) isotherms at −196 °C for a) PC*x*-K2 and b) PC450-K*y* samples.

Table 3
Textural properties of PC*x*-K*y* samples obtained from N_2-adsorption-isotherm measurements at -196 °C.

Sample	S_{BET} (m^2 g^{-1})	$S_{0.8}$[a] (m^2 g^{-1})	V_T[b] (cm^3 g^{-1})	V_m[c] (cm^3 g^{-1})	$V_{0.8}$[d] (cm^3 g^{-1})
PC300-K2	1405	1545	0.57	0.56	0.49
PC400-K2	1482	1518	0.60	0.59	0.49
PC450-K2	1675	1765	0.68	0.67	0.56
PC500-K2	1376	1482	0.56	0.55	0.47
PC600-K2	936	970	0.40	0.38	0.31
PC450-K1	1093	989	0.41	0.40	0.31
PC450-K3	2296	1010	1.00	0.84	0.33

[a] Cumulative surface area of narrow micropores less than 0.8 nm.
[b] Total pore volume at $P/P_0 \sim 0.99$.
[c] Micropore volume determined from the Dubinin-Radushkevich equation.
[d] Cumulative pore volume of narrow micropores less than 0.8 nm.

Table 3 summarizes the textural properties of the PC*x*-K*y* samples estimated from their N_2 adsorption isotherms at −196 °C, including the specific Brunauer-Emmett-Teller (BET) surface area (S_{BET}), surface area of narrow micropores less than 0.8 nm ($S_{0.8}$), total pore volume (V_T), micropore volume (V_m), and pore volume of narrow micropores less than 0.8 nm (V_{nm}). For a fixed KOH/PC mass ratio of 2 (PC*x*-K2), the textural-property values increased with increasing carbonization temperature from 300 to 450 °C, and then decreased with further increases in the carbonization temperature. The PC450-K2 sample exhibited the maximum specific surface area (1675 m^2 g^{-1}) and total pore volume (0.68 cm^3 g^{-1}). When the carbonization temperature was fixed at 450 °C (PC450-K*y*), the values of S_{BET}, V_T, and V_m increased on increasing the KOH/PC mass ratio from 1 to 3, but interestingly $S_{0.8}$ and $V_{0.8}$ exhibited maximum values at a KOH/PC mass ratio of 2. Increasing the amount of KOH utilized results in more carbon consumption and more micropore development according to the reaction $6KOH + 2C \rightarrow 2K + 3H_2 + 2K_2CO_3$ [45]. It appears that increasing the KOH/PC mass ratio not only results in more pore production, but also enlargement of the pore size, and this effect was most significant for narrow micropores. The pore structure of the porous carbon samples significantly depended on the KOH/PC mass ratio used in the adsorbent preparation process.

Pore size distributions for the samples were estimated from the N_2 adsorption isotherms using a non-local density-functional-theory (NLDFT) model assuming a heterogeneous surface, with the results shown in Fig. 5. The micropores were well developed in the PC*x*-K2 samples and the most of pore sizes were less than 0.8 nm, with a strong peak at 0.65 nm present for all PC*x*-K2 samples (Fig. 5a). The intensity of this peak as a function of carbonization temperature matches well with the trend of N_2 uptake displayed in Fig. 4a. Pore size distributions for the PC450-K*y* samples with varying KOH/PC mass ratio from 1 to 3 are shown in Fig. 5b. A strong peak at 0.65 nm is found for all PC450-K*y* samples; however, a new peak at 0.9 nm also appears in PC450-K3, indicating that the pore size increased on increasing the KOH/PC mass ratio to 3. All PC*x*-K*y* samples mainly possess narrow micropores of less than 1.0 nm and are, thus, likely to be effective CF_4 adsorbents [46,47].

3.2. CF_4 adsorption on KOH-activated PC

Fig. 6 shows CF_4 adsorption isotherms for the PC*x*-K*y* samples measured at 25 °C. Among the PC*x*-K2 samples, PC450-K2 (carbonized at 450 °C) exhibited the highest CF_4 uptake of 2.79 mol kg^{-1} at 25 °C and 1 atm (Fig. 6a). Increasing or decreasing the carbonization temperature from 450 °C reduced the CF_4 uptake; this behavior is consistent with the textual properties presented in Table 3. Also, the KOH/PC mass ratio was varied, with a constant carbonization temperature of 450 °C (PC450-K*y*), to investigate the effect of KOH/PC mass ratio on CF_4 adsorption (Fig. 6b). PC450-K2 exhibited higher CF_4 adsorption uptake than PC450-K1 and PC450-K3, indicating that the KOH/PC mass ratio should be optimized for achieving the highest CF_4 uptake. As seen in Table 3, the specific surface area and total pore volume increased with increasing KOH/PC mass ratio between 1 and 3; however, the CF_4 uptake showed a maximum at a specific KOH/PC mass ratio of 2. This indicates that the CF_4 uptake is not exclusively dependent on the specific surface area or total pore volume.

In order to study in detail the effects of the textural properties on CF_4 uptake, the relationships between the individual textural properties and the CF_4 uptake at 25 °C and 1 atm were plotted, as shown in Fig. 7. It is noticeable that the CF_4 uptake of the PC*x*-K*y* samples does not show a clear relationship with the specific surface area and total pore volume, but exhibits a linear trend with the surface area and pore volume of narrow micropores less than 0.8 nm, with correlation coefficients (R^2) higher than 0.98. Compared with the specific surface area and total pore volume, the surface area and pore volume of narrow micropores less than 0.8 nm appear to dominate the CF_4 uptake. This is attributed to the strong adsorption potential of narrow micropores and consequent increased interaction strength with CF_4 [48].

The CF_4 adsorption uptake exhibited by PC450-K2 in this study (2.79 mol kg^{-1}) is much higher than or comparable to previously reported values (Table 1). The highest CF_4 adsorption uptake reported previously was 2.96 mol kg^{-1} for a TiC-CDC800H sample [24]. However, the PC-derived porous carbon is a more viable candidate than TiC

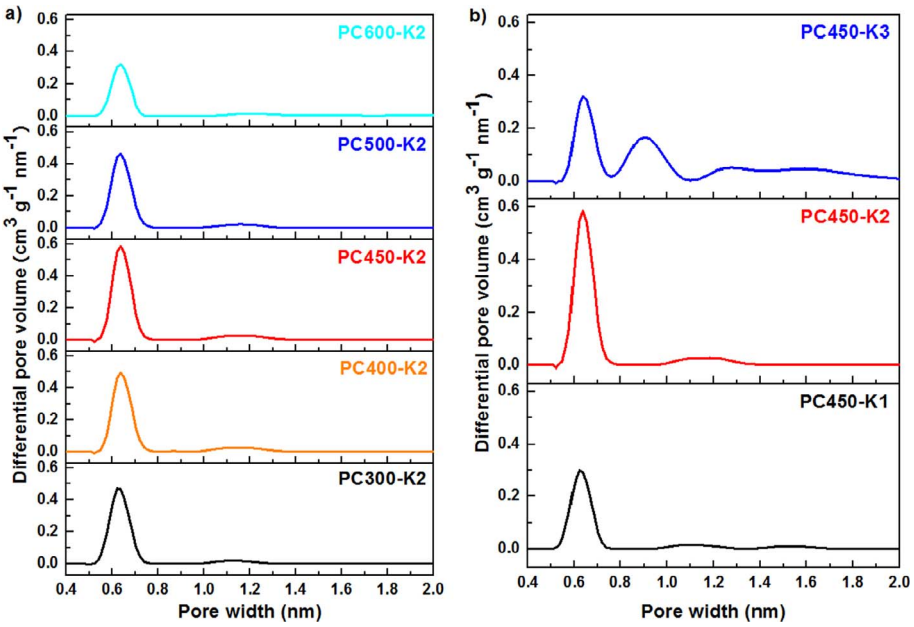

Fig. 5. Pore size distribution of a) PC*x*-K2 and b) PC450-K*y* samples.

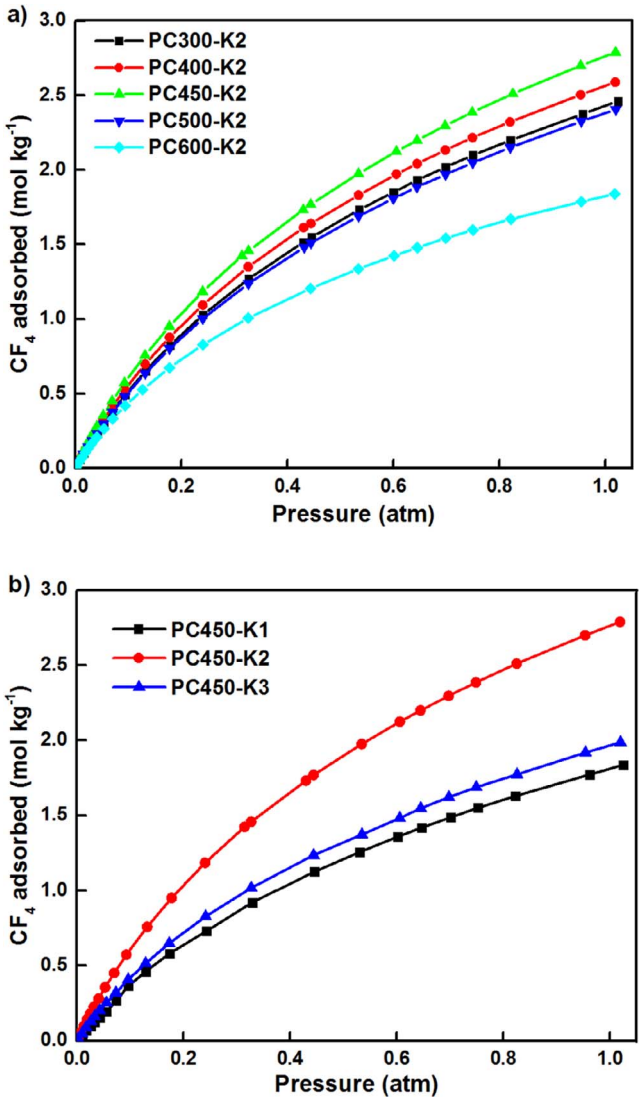

Fig. 6. CF_4 adsorption isotherms at 25 °C for a) PC*x*-K2 and b) PC450-K*y* samples.

powder-derived for CF_4 adsorption because of the cheap price of PC and its abundant production in oil refineries, and the lower-temperature sample preparation used here.

The CF_4 adsorption behavior of PC450-K2 was compared at three different temperatures (25, 40, and 60 °C), with the isotherms presented in Fig. 8. The CF_4 uptake of PC450-K2 sample reached 2.79, 2.13, and 1.45 mol kg^{-1} under atmospheric pressure at 25, 40, and 60 °C, respectively. This decrease in CF_4 uptake with increasing adsorption temperature indicates that exothermic physisorption governs the CF_4 adsorption process [24]. The adsorption data were fitted using the Langmuir-isotherm model (Eq. (1)) [49,50], where q_e is the amount adsorbed at each equilibrium point, q_{max} is the maximum adsorption uptake (mol kg^{-1}), K_L is the Langmuir constant, and p is the pressure (atm). The model parameters are listed in Table 4. The adsorption experimental data were well fitted by the Langmuir-isotherm model, with R^2 values of greater than 0.99. The estimated CF_4 adsorption (q_{max}) reaches 4.65 mol kg^{-1} under 25 °C and 1 atm.

$$q_e = \frac{q_{max} K_L p}{1 + K_L p} \quad (1)$$

3.3. Kinetic study on CF_4 adsorption by PC450-K2

Studying the adsorption equilibrium is important for determining the effectiveness of adsorption. However, it is also necessary to identify the type of adsorption mechanism and kinetic behavior in any given system. In this study, three different models (pseudo-seconder-order kinetic model, Elovich model, and intra-particle diffusion model) were used to predict the adsorption kinetics of CF_4 on PC450-K2.

The widely used pseudo-second-order kinetic equation is expressed in Eq. (2).

$$\frac{t}{q_t} = \frac{1}{k_2 q_e^2} + \frac{t}{q_e} \quad (2)$$

where k_2 is the rate constant of pseudo-second-order adsorption and q_t is the amount adsorbed at a specific time (t), and the initial adsorption rate (h) is expressed as follows:

$$h = k_2 q_e^2 \quad (3)$$

The Elovich model has also been used successfully to describe second-order kinetic processes and has been applied satisfactorily to

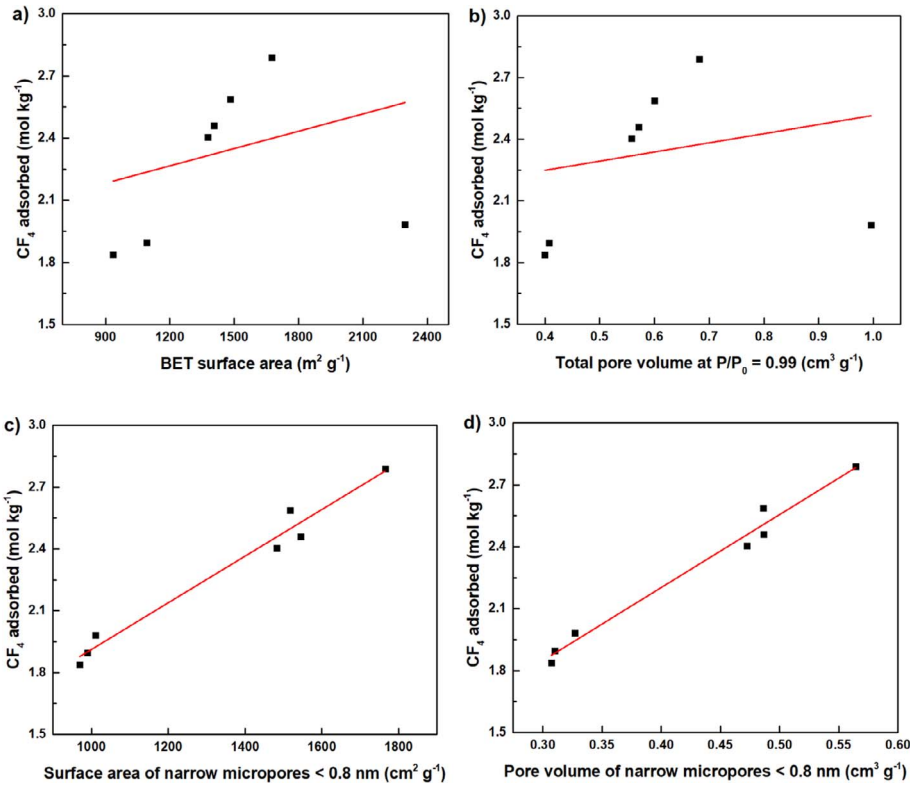

Fig. 7. Plots of CF_4 uptake (at 25 °C and 1 atm) as a function of the PC*x*-K*y* textural properties.

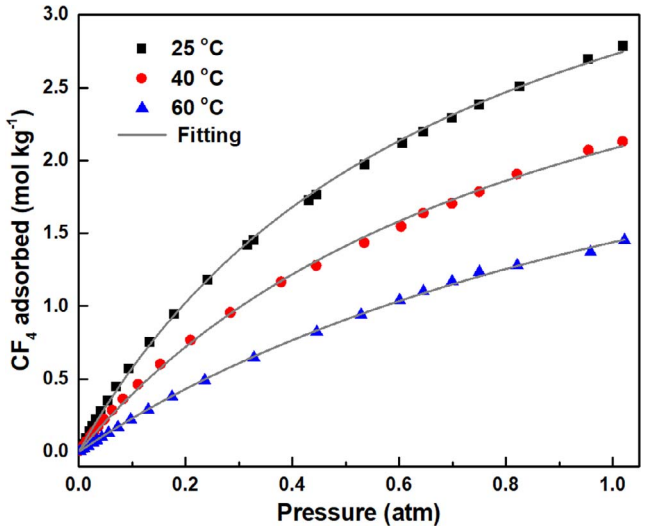

Fig. 8. CF_4 adsorption isotherms for PC450-K2 at 25, 40, and 60 °C. The dots and the solid lines represent experimental data and Langmuir model fittings, respectively.

Table 4
Langmuir model fitting parameters for CF_4 adsorption on PC450-K2.

Temperature (°C)	q_{max} (mol kg^{-1})	K_L (atm^{-1})	H ($=q_{max} \times K_L$) (mol kg^{-1} atm^{-1})	R^2
25	4.65	1.41	6.56	0.999
40	3.94	1.12	4.41	0.999
60	3.25	0.71	2.31	0.999

some chemisorption data. The Elovich equation is often valid for systems in which the adsorbing surface is heterogeneous, and the equation is formulated as shown in Eq. (4), where a_e is the initial adsorption rate, and b_e is related to the extent of surface coverage and activation energy for chemisorption.

$$q_t = \frac{\ln a_e b_e}{b_e} + \frac{1}{b_e}\ln t \tag{4}$$

The intra-particle diffusion model identifies diffusion mechanisms, and kinetic results are analyzed using Eq. (5), where C is the intercept and k_i is the intra-particle diffusion rate constant.

$$q_t = k_i t^{1/2} + C \tag{5}$$

To justify the validity of kinetic models, root mean square error (RMSE) was calculated as follows [51]:

$$\mathrm{RMSE} = \left(\frac{\sum (q_{exp} - q_{cal})^2}{N} \right)^{1/2} \tag{6}$$

where q_{exp} and q_{cal} represent the experimental and calculated values and N is the number of measurements. The lower value of RMSE indicates the better fitting.

Fig. 9 shows kinetic data for CF_4 adsorption on PC450-K2 and fits using the three different kinetic models, with the parameters obtained from fitting the kinetic models at 30, 40, and 60 °C shown in Table 5. The CF_4 adsorption kinetic data were reproducible and reliable in the measurement using TGA. The pseudo-second-order model best fitted the experimental data, showing R^2 values of ~1 and the lowest RMSE values. The initial adsorption rate (h), determined from fitting with the pseudo-second-order model, decreases with increasing temperature. The Elovich model cannot be used to describe the CF_4 adsorption process because the initial adsorption rate (a_e) in the first few minutes is significantly greater than q_e obtained from the experimental data. The adsorption rate was initially very rapid and then slowed after a few minutes, indicating that the CF_4 molecules adsorbed on the easily accessible surface of large outer pores first and then adsorbed on the surface of small inner pores; this process was mainly controlled by diffusion.

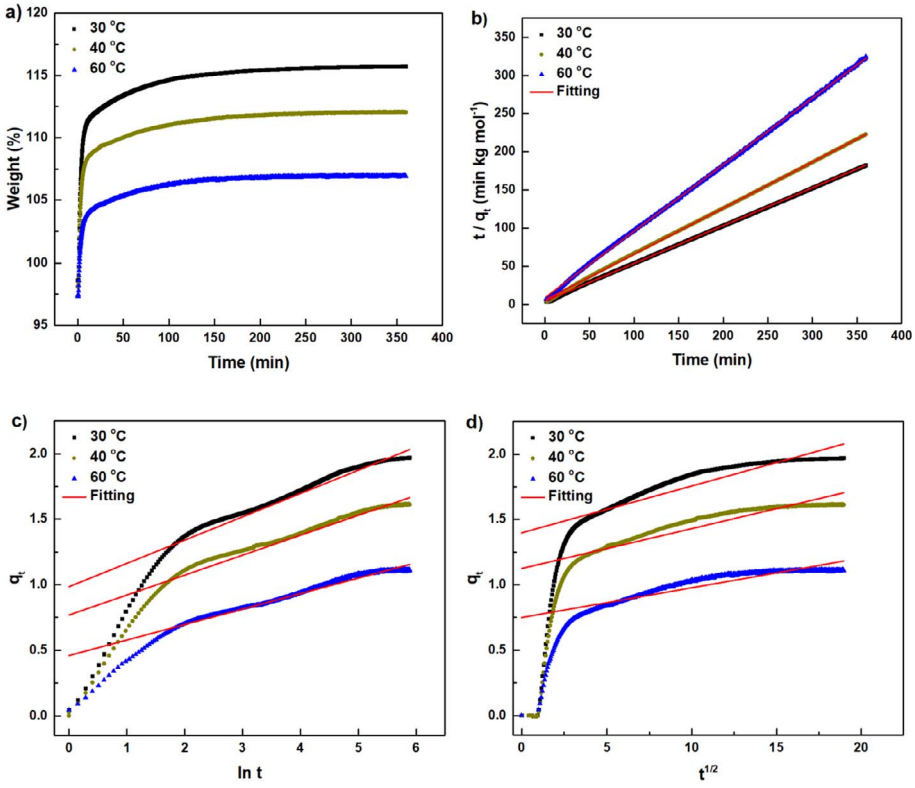

Fig. 9. a) Kinetic data for CF_4 adsorption on PC450-K2, and fittings using b) the pseudo-second-order-adsorption kinetic model, c) the Elovich adsorption kinetic model, and d) the intra-particle-adsorption kinetic model.

Table 5
Parameters of three kinetic models for CF_4 adsorption on PC450-K2.

Model	Parameter	Temperature (°C)		
		30	40	60
Experimental data	q_e (mol kg^{-1})	2.79	2.13	1.45
Second-order model	k_2 (kg mol^{-1} min^{-1})	0.061	0.066	0.088
	q_e (mol kg^{-1})	2.02	1.66	1.15
	h (mol kg^{-1} min^{-1})	0.246	0.182	0.116
	R^2	0.999	0.999	0.999
	RMSE	0.041	0.042	0.034
Elovich model	a_e (mol kg^{-1} min^{-1})	45.166	23.434	5.755
	b_e (kg mol^{-1})	5.622	6.551	8.460
	R^2	0.891	0.901	0.932
	RMSE	0.072	0.055	0.035
Intra-particle diffusion model	k_i (kg mol^{-1} min$^{-1/2}$)	0.036	0.031	0.023
	C	1.398	1.125	0.749
	R^2	0.617	0.647	0.726
	RMSE	0.123	0.098	0.071

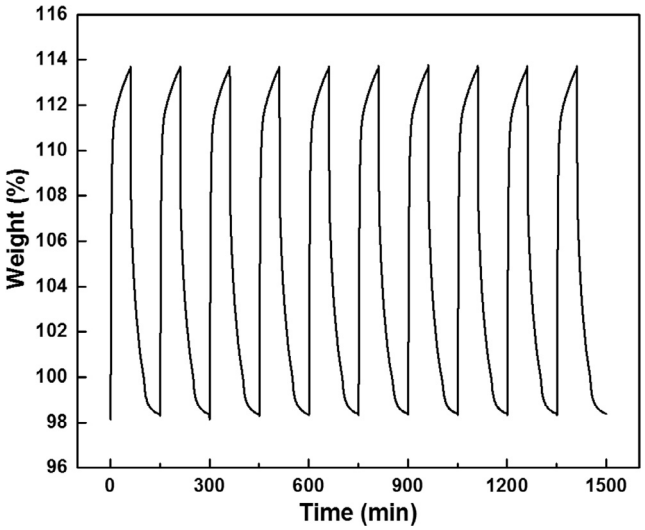

Fig. 10. Cyclic test of CF_4 adsorption-desorption using PC450-K2.

3.4. Cyclic stability and selectivity of PC450-K2

Fig. 10 shows the results of a cyclic stability test for CF_4 adsorption-desorption on PC450-K2 using TGA. A stable working uptake of 1.79 mol kg^{-1} was well maintained with fast adsorption-desorption kinetics over ten repetitive cycles. It is noteworthy that the adsorbent was easily regenerated with a simple N_2 purge. Because CF_4 is usually vented with a large amount of N_2, the selectivity of CF_4 over N_2 is another crucial factor when developing CF_4 adsorbents. To estimate the CF_4/N_2 selectivity, the N_2 adsorption isotherm of PC450-K2 was measured at 25 °C using the same volumetric adsorption analyzer used to measure the CF_4 adsorption isotherm (Section 3.2). The adsorption selectivity ($S_{i,j}$) was calculated using the ideal adsorbed solution theory (IAST) from two single-component CF_4 and N_2 isotherms, as described in Eq. (7), where Q_i and p_i are the adsorption uptake and partial pressure of component i, respectively [52].

$$S_{i,j} = \frac{Q_i/p_i}{Q_j/p_j} \tag{7}$$

In the calculation, it was assumed that only N_2 and CF_4 were involved and the sum of the partial pressures of N_2 and CF_4 was equal to 1 atm. The calculated IAST selectivity was in the range of 6–15, and decreased with increasing CF_4 partial pressure (Fig. 11), mainly due to the saturation of potential adsorption sites. The CF_4 concentrations in commercial industry are low (generally in the range of ~ 500 to a few-thousand ppm [53]), therefore the high selectively for CF_4 over N_2 at low CF_4 partial pressures clearly shows that PC450-K2 is advantageous for selective CF_4 capture.

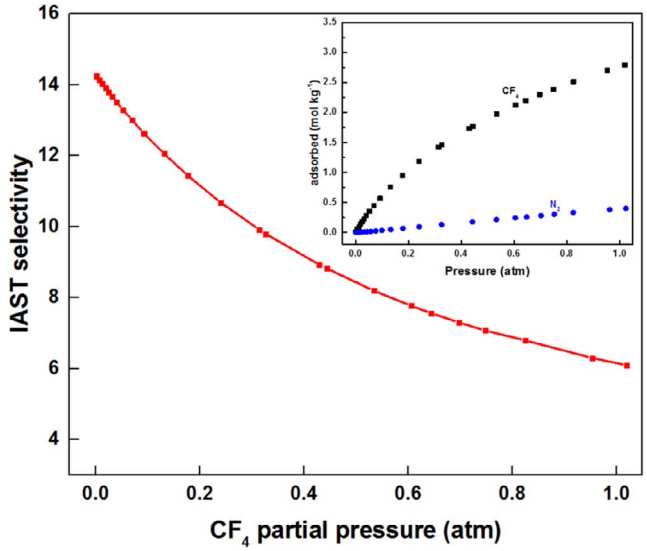

Fig. 11. IAST selectivity of PC450-K2 toward CF_4 over N_2 at 25 °C.

4. Conclusions

Microporous carbon adsorbents were prepared using KOH activation of petroleum coke (PC), and used to capture CF_4 gas, which is a significant global warming compound. The carbonization temperature and KOH/PC mass ratio used in sample preparation were varied in the range of 300–600 °C and 1–3, respectively, and their effects on the physical characteristics and CF_4-adsorption performance of the PC-based microporous carbons (PC*x*-K*y*) were investigated. The textural properties of the PC*x*-K*y* samples varied significantly as a function of the carbonization temperature and KOH/PC mass ratio. The specific surface area and total pore volume peaked at a carbonization temperature of 450 °C, but increased continually with increasing KOH/PC mass ratio. Interestingly, the surface area and pore volume of narrow micropores peaked at a carbonization temperature and KOH/PC mass ratio of 450 °C and 2, respectively. The experimental CF_4-adsorption data were well fitted by the Langmuir isotherm model, and the PC450-K2 sample exhibited the highest CF_4 adsorption uptake of 2.79 mol kg^{-1} at 25 °C and 1 atm. The CF_4 adsorption uptake of PC*x*-K*y* was remarkably dominated by the surface area and pore volume of narrow micropores below 0.8 nm in size. The pseudo-second-order kinetic model matched well with the experimental CF_4-adsorption data, while the Elovich and intra-particle diffusion kinetic models did not. It also appeared that CF_4 adsorption on PC*x*-K*y* is mainly controlled by physisorption rather than chemisorption. In addition to the high CF_4 adsorption uptake, PC450-K2 displayed good CF_4/N_2 selectivity at relatively low pressures, excellent recyclability, easy regeneration, and rapid adsorption-desorption kinetics.

Acknowledgement

This work was supported by the R&D Center for Reduction of Non-CO_2 Greenhouse Gases (2013001690013) as the Global Top Environment R&D Program and by the "Public Technology Program based on Environment Policy" (Grant number E416-00070-0604-0). Both programs were funded by the Korean Ministry of Environment (MOE).

References

[1] S.W. Choi, S.-M. Hong, J.-H. Park, H.T. Beum, K.B. Lee, CF_4 Adsorption on microporous carbons prepared by carbonization of poly(vinylidene fluoride), Ind. Eng. Chem. Res. 54 (2015) 8561–8568.
[2] N. MacDowell, N. Florin, A. Buchard, J. Hallett, A. Galindo, G. Jackson, C.S. Adjiman, C.K. Williams, N. Shah, P. Fennell, An overview of CO_2 capture technologies, Energy Environ. Sci. 3 (2010) 1645–1669.
[3] S.-M. Hong, S.W. Choi, S.H. Kim, K.B. Lee, Porous carbon based on polyvinylidene fluoride: enhancement of CO_2 adsorption by physical activation, Carbon 99 (2016) 354–360.
[4] D.A. Sekiya, D.R. Ahuja, Relative contributions of greenhouse gas emissions to global warming, Nature 344 (1990) 529–531.
[5] H.J. Jang, S. Kim, K.B. Lee, Simplified synthesis of K_2CO_3-promoted hydrotalcite based on hydroxide-form precursors: effect of Mg/Al/K_2CO_3 ratio on high-temperature CO_2 sorption capacity, Korean J. Chem. Eng. 34 (2017) 1–5.
[6] S.I. Garcés-Polo, J. Villarroel-Rocha, K. Sapag, S.A. Korli, A. Gil, A comparative study of CO_2 diffusion from adsorption kinetic measurements on microporous material at low pressures and temperatures, Chem. Eng. J. 302 (2016) 278–286.
[7] D.M. D'Alessandro, B. Smith, J.R. Long, Carbon dioxide capture: prospects for new materials, Angew. Chem. Int. Edit. 49 (2010) 6058–6082.
[8] J. Wang, L. Huang, R. Yang, Z. Zhang, J. Wu, Y. Gao, Q. Wang, D. O'Hare, Z. Zhong, Recent advances in solid sorbents for CO_2 capture and new development trend, Energy Environ. Sci. 7 (2014) 3478–3518.
[9] B.P. Spigarelli, S. Komar Kawatra, Opportunities and challenges in carbon dioxide capture, J. CO_2 Util. 1 (2013) 69–87.
[10] W.Q. Liu, H. An, C.L. Qin, J.J. Yin, G.X. Wang, B. Feng, M.H. Xu, Performance enhancement of calcium oxide sorbents for cyclic CO2 capture-A review, Energy Fuels 26 (2012) 2751–2767.
[11] A. Samanta, A. Zhao, G.K.H. Shimizu, P. Sarkar, R. Gupta, Post-combustion CO_2 capture using solid sorbents: A review, Ind. Eng. Chem. Res. 51 (2012) 1438–1463.
[12] H.Q. Yang, Z.H. Xu, M.H. Fan, R. Gupta, R.B. Slimane, A.E. Bland, I. Wright, Progress in carbon dioxide separation and capture: A review, J. Environ. Sci. 20 (2008) 14–27.
[13] S.A. Montzka, E.J. Dlugokencky, J.H. Butler, Non-CO_2 greenhouse gases and climate change, Nature 476 (2011) 43–50.
[14] M.-K. Moon, U.-W. Nam, C.-H. Lee, V.T. Em, Y.-H. Choi, J.-K. Cheon, K.-N. Kong, Low efficiency 2-dimensional position-sensitive neutron detector for beam profile measurement, Nucl. Instrum. Methods Phys. Res. A 538 (2005) 592–596.
[15] J. Kim, P.J. Fraser, S. Li, J. Muhle, A.L. Ganesan, P.B. Krummel, L.P. Steele, S. Park, S.-K. Kim, M.-K. Park, T. Arnold, C.M. Harth, P.K. Salameh, R.G. Prinn, R.F. Weiss, K.-R. Kim, Quantifying aluminum and semiconductor industry perfluorocarbon emissions from atmospheric measurements, Geophys. Res. Lett. 41 (2014) 4787–4794.
[16] S. Singh, F. Tezel, P.J.E. Harlick, Adsorption of tetrafluoromethane and nitrogen by various adsorbents, Sep. Sci. Technol. 37 (2002) 2763–2784.
[17] S. Lee, J.W. Choi, S.-H. Lee, Separation of greenhouse gases (SF_6, CF_4 and CO_2) in an industrial flue gas using pilot-scale membrane, Sep. Purif. Technol. 148 (2015) 15–24.
[18] IPCC's Fourth Assessment Report-Errata (IPCC 2012), http://www.ipcc.ch/report/ar4/wg1/.
[19] S. Furmaniak, A.P. Terzyk, P.A. Gauden, P. Kowalczyk, P.J.F. Harris, S. Koter, Applicability of molecular simulations for modeling the adsorption of the greenhouse gas CF_4 on carbons, J. Phys.: Condens. Matter 25 (2013) 015004.
[20] Y. Boyjoo, Y. Cheng, H. Zhong, H. Tian, J. Pan, V.K. Pareek, S.P. Jiang, J.-F. Lamonier, M. Jaroniec, J. Liu, From waste Coca Cola® to activated carbons with impressive capabilities for CO_2 adsorption and supercapacitors, Carbon 116 (2017) 490–499.
[21] B.B. Saha, K.Ch. Ng, Advances in adsorption technology-Chapter 15, Nova Sci. (2010) 1–34.
[22] M.G. Plaza, A.S. González, J.J. Pis, F. Rubiera, C. Pevida, Production of microporous biochars by single-step oxidation: effect of activation conditions on CO_2 capture, Appl. Energy 114 (2014) 551–562.
[23] A. Heidari, H. Younesi, A. Rashidi, A. Ghoreyshi, Adsorptive removal of CO_2 on highly microporous activated carbons prepared from Eucalyptus camaldulensis wood: effect of chemical activation, J. Taiwan Inst. Chem. E. 45 (2014) 579–588.
[24] S.W. Choi, D.-H. Lee, J.H. Kim, J.Y. Kim, J.-H. Park, H.T. Beum, D.-S. Lim, K.B. Lee, A titanium carbide-derived novel tetrafluoromethane adsorbent with outstanding adsorption performance, Chem. Eng. J. 311 (2017) 227–235.
[25] J. Jagiello, T.J. Bandosz, K. Putyera, J.A. Schwarz, Adsorption near ambient temperatures of Methane, carbon tetrafluoride, and sulfur hexafluoride on commercial activated carbons, J. Chem. Eng. Data 40 (1995) 1288–1292.
[26] E. Senkovska, J.A.R. Barea, S. Navarro, Kaskel, Adsorptive capturing and storing greenhouse gases such as sulfur hexafluoride and carbon tetrafluoride using metal-organic frameworks, Microporous Mesoporous Mater 156 (2012) 115–120.
[27] R.K. Motkuri, H.V.R. Annapureddy, M. Vijaykumar, H.T. Schaef, P.F. Martin, B.P. McGrail, L.X. Dang, R. Kroshna, P.K. Thallapally, Fluorocarbon adsorption in hierarchical porous frameworks, Nat. Commun. 5 (2014) 4368.
[28] P. Kowalczyk, R. Holyst, Efficient adsorption of super greenhouse gas (tetrafluoromethane) in carbon nanotubes, Environ. Sci. Technol. 42 (2008) 2931–2936.
[29] N.-G. Ahn, S.-W. Kang, B.-H. Min, S.-S. Suh, Adsorption isotherms of tetrafluoromethane and hexafluoroethane on various adsorbents, J. Chem. Eng. Data 51 (2006) 451–456.
[30] S. Singh, F.H. Rezel, P.J.E. Harlick, Adsorption of tetrafluoromethane and nitrogen by various adsorbents, Sep. Sci. Technol. 37 (2002) 2763–2784.
[31] Y. Li, T. Ben, B. Zhang, Y. Fu, S. Qiu, Ultrahigh gas storage both at low and high pressures in KOH-activated carbonized porous aromatic frameworks, Sci. Rep. 3 (2013) 2420.
[32] M. Choi, R. Ryoo, Mesoporous carbons with KOH activated framework and their hydrogen adsorption, J. Mater. Chem. 17 (2007) 4204–4209.
[33] Y.P. Guo, D.A. Rockstraw, Physical and chemical properties of carbons synthesized from xylan, cellulose, and Kraft lignin by H3PO4 activation, Carbon 44 (2006)

1464–1475.
[34] R.L. Xiao, S.P. Xu, Q.X. Li, Y.M. Su, The effects of hydrogen on KOH activation of petroleum coke, J. Anal. Appl. Pyrol. 96 (2012) 120–125.
[35] Y. Zhang, X.J. Li, J.F. Huang, W. Xing, Z.F. Yan, Functionalization of petroleum coke-derived carbon for synergistically enhanced capacitive performance, Nanoscale Res. Lett. 11 (2016) 163.
[36] C.L. Lu, S.P. Xu, Y.X. Gan, S.Q. Liu, C.H. Liu, Effect of pre-carbonization of petroleum cokes on chemical process with KOH, Carbon 43 (2005) 2295–2301.
[37] Y. Chen, B. Huang, B. Cai, On the preparation and characterization of activated carbon from mangosteen shell, J. Taiwan Inst. Chem. E. 42 (2011) 837–842.
[38] E. Fuente, J.A. Menendez, M.A. Diez, D. Suarez, M.A. Montes-Moran, Infrared spectroscopy of carbon materials: A quantum chemical study of model compounds, J. Phys. Chem. B 107 (2003) 6350–6359.
[39] Y.L. Wang, B.B. Chang, D.X. Guan, X.P. Dong, Mesoporous activated carbon spheres derived from resorcinol-formaldehyde resin with high performance for supercapacitors, J Solid State Electrochem. 19 (2015) 1783–1791.
[40] D. Cuhadaroglu, O.A. Uygun, Production and characterization of activated carbon from a bituminous coal by chemical activation, Afr. J. Biotechnol. 7 (2008) 3703–3710.
[41] Z. Li, Z.W. Xu, X.H. Tan, H.L. Wang, C.M.B. Holt, T. Stephenson, B.C. Olsen, D. Mitlin, Mesoporous nitrogen-rich carbons derived from protein for ultra-high capacity battery anodes and supercapacitors, Energy Environ. Sci. 6 (2013) 871–878.
[42] H. Kim, H. Cho, S.Y. Jang, Y.W. Song, Deformation-immunized optical deposition of graphene for ultrafast pulsed lasers, Appl. Phys. Lett. 98 (2011) 021104.
[43] J.D. Xu, Q.M. Gao, Y.L. Zhang, Y.L. Tan, W.Q. Tian, L.H. Zhu, L. Jiang, Preparing two-dimensional microporous carbon from Pistachio nutshell with high areal capacitance as supercapacitor materials, Sci. Rep. 4 (2014) 5545.
[44] E. Robens, F. Rouquerol, J. Rouquerol, K. Sing, Adsorption by Powders and Porous Solids, Academic Press, London, UK, 1999.
[45] M.A. Lillo-Ródenas, D. Cazorla-Amorós, A. Linares-Solano, Understanding chemical reactions between carbons and NaOH and KOH: an insight into the chemical activation mechanism, Carbon 41 (2003) 267–275.
[46] X. Hu, M. Radosz, K.A. Cychosz, M. Thommes, CO_2-filling capacity and selectivity of carbon nanopores: synthesis, texture, and pore-size distribution from quenched-solid density functional theory (QSDFT), Environ. Sci. Technol. 45 (2011) 7068–7074.
[47] M. Sevilla, C. Falco, M.-M. Titirici, A.B. Fuertes, High-performance CO_2 sorbents from algae, RSC Adv. 2 (2012) 12792–12797.
[48] M. Sevilla, A.B. Fuertes, Sustainable porous carbons with a superior performance for CO_2 capture, Energy Environ. Sci. 4 (2011) 1765–1771.
[49] J.A. Mason, K. Sumida, Z.R. Herm, R. Krishna, J.R. Long, Evaluating metal-organic frameworks for post-combustion carbon dioxide capture via temperature swing adsorption, Energy Environ. Sci. 4 (2011) 3030–3040.
[50] K.Y. Foo, B.H. Hameed, Insights into the modeling of adsorption isotherm systems, Chem. Eng. J. 156 (2010) 2–10.
[51] R. Beigzadeh, M. Hajialyani, M. Rahimi, Heat transfer and fluid flow modeling in serpentine microtubes using adaptive neuro-fuzzy approach, Korean J. Chem. Eng. 33 (2016) 1534–1550.
[52] B. Liu, B. Smit, Comparative molecular simulation study of CO_2/N_2 and CH_4/N_2 separation in zeolites and metal-organic frameworks, Langmuir 25 (2009) 5918–5926.
[53] H. Imamura, Apparatus for Removing Harmful Components in a Semiconductor Exhaust Gas, US 6,126,906 A, Kanken Techno Co., Ltd, Japan, 2000.